Inhibition of Osteoclast Differentiation by Gold Nanoparticles Functionalized with Cyclodextrin Curcumin Complexes

Dong Nyoung Heo,[†,#] Wan-Kyu Ko,[†,#] Ho-Jin Moon,[†] Han-Jun Kim,[∥] Sang Jin Lee,[†] Jung Bok Lee,[†] Min Soo Bae,[†] Jin-Kyu Yi,[‡] Yu-Shik Hwang,[†] Jae Beum Bang,[§] Eun-Cheol Kim,[⊥] Sun Hee Do,[*,∥] and Il Keun Kwon[*,†]

[†]Department of Maxillofacial Biomedical Engineering and Institute of Oral Biology, School of Dentistry, [‡]Department of Conservative Dentistry, School of Dentistry, [§]Department of Dental Education, School of Dentistry, and [⊥]Department of Maxillofacial Tissue Regeneration, School of Dentistry and Research Center for Tooth and Periodontal Regeneration (MRC), Kyung Hee University, Seoul 130-701, Republic of Korea and [∥]Department of Clinical Pathology, College of Veterinary Medicine, Konkuk University, Seoul 143-701, Republic of Korea. [#]These authors contributed equally to this work.

ABSTRACT Gold nanoparticles (GNPs) have been previously reported to inhibit osteoclast (OC) formation. However, previous research only confirmed the osteoclastogenesis inhibitory effect under *in vitro* conditions. The aim of this study was to develop a therapeutic agent for osteoporosis based on the utilization of GNPs and confirm their effect both *in vitro* and *in vivo*. We prepared β-cyclodextrin (CD) conjugated GNPs (CGNPs), which can form inclusion complexes with curcumin (CUR—CGNPs), and used these to investigate their inhibitory effects on receptor activator of nuclear factor-κb ligand (RANKL)-induced osteoclastogenesis in bone marrow-derived macrophages (BMMs). The CUR—CGNPs significantly inhibited the formation of tartrate-resistant acid phosphatase (TRAP)-positive multinuclear cells in BMMs without inducing cytotoxicity. The mRNA expressions of genetic markers of OC differentiation including c-Fos, nuclear factor of activated T cells 1 (NFATc1), TRAP, and osteoclast associated receptor (OSCAR) were significantly decreased in the presence of CUR—CGNPs. In addition, the CUR—CGNPs inhibited OC differentiation of BMMs through suppression of the RANKL-induced signaling pathway. Additionally, CUR—CGNPs caused a decrease in RANKL-induced actin ring formation, which is an essential morphological characteristic of OC formation allowing them to carry out bone resorption activity. Furthermore, the *in vivo* results of an ovariectomy (OVX)-induced osteoporosis model showed that CUR—CGNPs significantly improved bone density and prevented bone loss. Therefore, CUR—CGNPs may prove to be useful as therapeutic agents for preventing and treating osteoporosis.

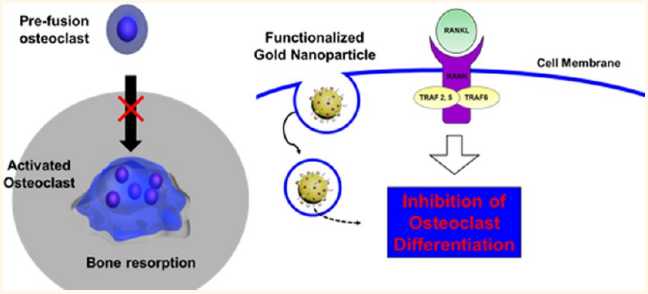

KEYWORDS: gold nanoparticles · osteoclast differentiation · curcumin · osteoporosis RANK signaling

Over the past few decades, nanotechnology has demonstrated the capability of inorganic-based nanoparticles (NPs) to be applied to a wide variety of medical applications including drug, protein and gene delivery, cell targeting, imaging, diagnostics, and tissue engineering.[1−3] Various inorganic NPs have been considered for usage in a broad range of biomedical applications due to their unique chemical and biological properties.

In recent years, a number of researchers have reported that various inorganic NPs could enhance osteoblastogenesis.[4−10] It was notably found that gold nanoparticles (GNPs) enhance the proliferation and osteogenic differentiation of cells in a dose- and size-dependent manner by their cellular interactions.[4−6] Well-dispersed carbon nanotubes and poly(lactic-*co*-glycolic acid) (PLGA) reinforced with carbon nanotubes have also demonstrated a capacity to promote osteoblastogenesis.[7,8] Akhavan *et al.* described that human mesenchymal stem cells (hMSCs) cultured on two-dimensional nanopatterned templates with graphene oxide showed a higher actin cytoskeletal proliferation and differentiation toward osteoblasts than control.[9] Yang *et al.* reported that metallofullerene NPs promoted

* Address correspondence to shdo@kokkuk.ac.kr, kwoni@khu.ac.kr.

Received for review June 25, 2013 and accepted November 24, 2014.

Published online November 24, 2014
10.1021/nn504329u

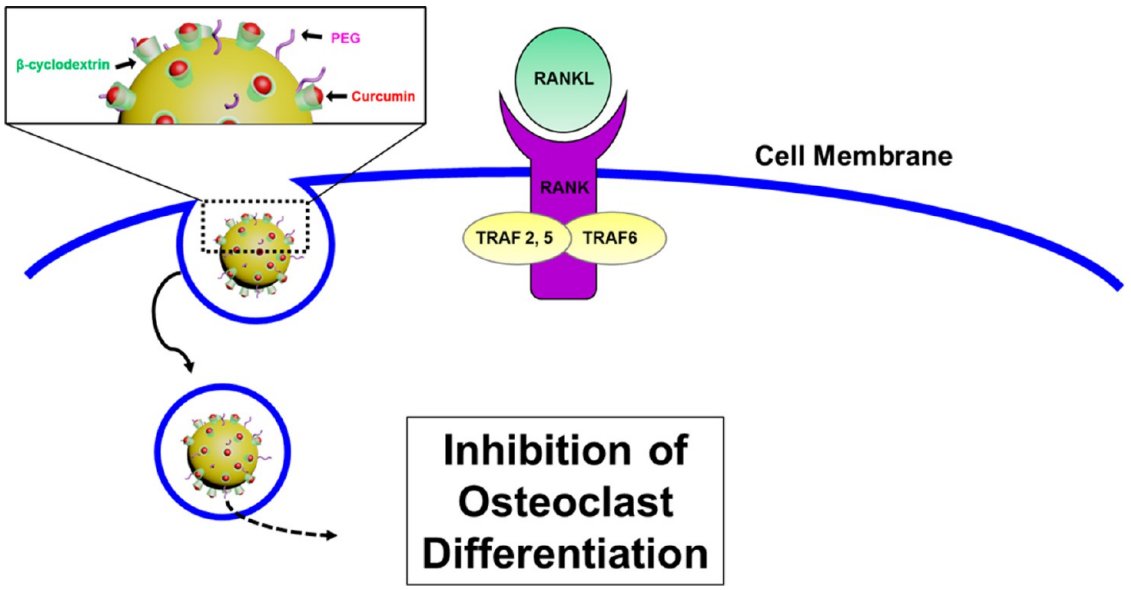

Figure 1. Schematic diagram of functionalized GNPs covered with CD/CUR inclusion complexes and their application for preventing osteoporosis.

osteoblastogenesis and improved bone mineral density *in vivo*.[10] In this regard, it was found that inorganic-based NPs can significantly affect osteogenic differentiation by intracellular interaction with nanosized materials.

Furthermore, inorganic-based NPs can affect osteoclast (OC) differentiation.[11−13] OC differentiation should be the most important evaluation point because it is directly involved in bone tissue remodeling. Bone tissue is remodeled through the balanced action of bone formation by osteoblasts and bone resorption by OCs. Bone resorption is necessary to maintain homeostasis for bone remodeling, but excessive resorption leads to osteoporosis. Excessive bone resorption is mostly caused by increased OC formation.[14,15] Therefore, the inhibition of OC formation is necessary for preventing osteoporosis. Sul *et al.* demonstrated that GNPs inhibit the receptor activator of nuclear factor-κb ligand (RANKL) and reduce the reactive oxygen species (ROS) levels in bone marrow-derived macrophages (BMMs).[11] Kim *et al.* found that platinum NPs suppress RANKL-induced OC formation by impairing RANKL signaling.[12] Beck *et al.* reported that silica-based NPs stimulated osteoblastogenesis, suppressed osteoclastogenesis, and enhanced overall bone mineral density *in vivo*.[13]

Among the various studied inorganic-based NPs, GNPs have been shown to be the most suitable material for bone tissue engineering applications because of their potential use in both inhibition of OC differentiation and stimulation of osteoblast formation. In addition, GNPs can be easily functionalized with biological molecules through well-established monolayer chemistry based on gold−thiol bonds.[16−18] Previously, we reported on a preparation of β-cyclodextrin (CD) surface-functionalized GNPs (CGNPs) and confirmation of its effects.[19] It is also possible to load paclitaxel, a hydrophobic drug, with CD on the GNPs surface by inclusion complex interactions. The GNPs covered with CD/paclitaxel inclusion complexes were well-dispersed in water-based solutions and effectively delivered the drug into the cells. Furthermore, CD-covered NPs work well as effective carriers of genes, proteins, drugs, and other molecules.[19−22]

Curcumin (CUR) has a wide range of pharmacological applications such as antiangiogenic, anti-inflammatory, antimicrobial, antioxidant, antiparasitic, antimutagenic, and anticancer properties.[23−25] CUR has been reported to show inherent green fluorescence property which can be used in potential application with fluorescence-based detection methods.[26−29] CUR is also known for its inhibitory effects on osteoclastogenesis and preventing osteoporosis by blocking RANKL-induced nuclear factor kappa B (NF-κB).[30,31] However, CUR has several drawbacks for clinical applications due to its low aqueous solubility, rapid degradation at physiological pH, and photodegradation in organic solvents.[26,32,33] To improve its water solubility, stability, and bioavailability, CDs are used as solubilizing and stabilizing agents for CUR through the formation of inclusion complexes.[23,26−28,32−34]

In view of the importance of the above studies, we prepared GNPs covered with CD/CUR inclusion complex (CUR−CGNPs) and investigated the inhibitory effect of this CUR−CGNPs on OC formation through intracellular uptake into the BMMs (Figure 1). CD-modified GNPs were prepared and used as carriers of CUR.

We additionally analyzed the function of CUR−CGNPs on bone tissue metabolism *in vivo*. We found that CUR−CGNPs act as RANKL-mediated osteoclastogenesis inhibitors in BMMs by reducing the activation of RANKL-induced signaling pathways. This action

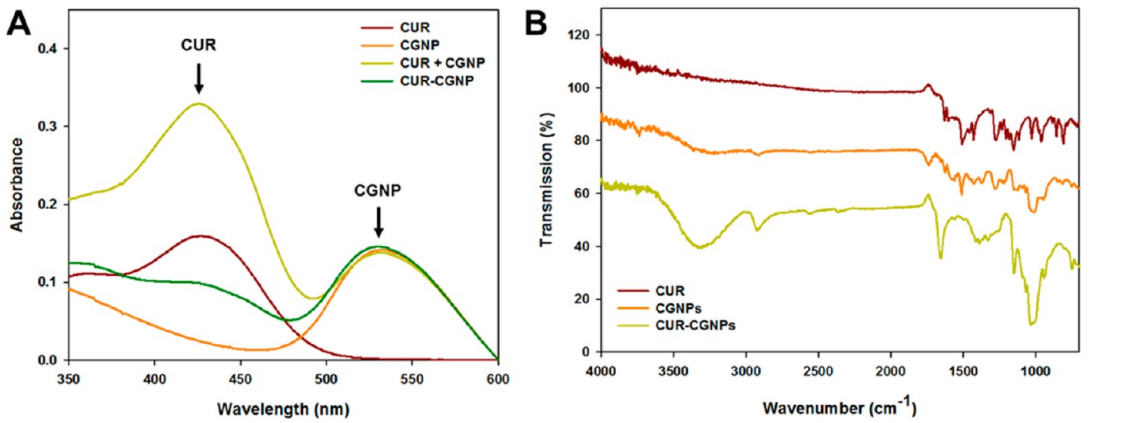

Figure 2. (A) Surface plasmon absorption spectra of mixed solutions with CGNP and CUR and (B) FTIR of CUR, CGNPs, and CUR−CGNPs. Spectra of solid powders were recorded by ATR-FTIR.

leads to a down regulation of transcriptional regulators such as c-Fos and nuclear factor of activated T cells 1 (NFATc1) and osteoclastogenic genes such as tartrate-resistant acid phosphatase (TRAP) and osteoclast associated receptor (OSCAR). In addition, CUR−CGNPs strongly reduced RANKL-induced p38, ERK, JNK, and IκBα activation and effectively prevented ovariectomy-induced bone loss *in vivo*.

RESULTS

Preparation and Characterization of CUR−CGNP. CGNPs were prepared by conjugating thiolated CD as a drug pocket and methoxy poly(ethylene glycol thiol) as a solvated antifouling shell on the surface of GNPs *via* Au−S bonds.[19] CUR was loaded onto the surface of the CGNPs by formation of inclusion complex. This design allows for efficient delivery of the CUR after intracellular uptake. The loading efficiency of CUR into CGNPs was measured by comparison of UV absorptions of CUR between the CUR solution for the incubation with CGNPs and the supernatant after purification by ultracentrifugation (Figures S1 and S2, Supporting Information). The approximate loading efficiency of CUR was 38.95%, and the concentrations of CUR−CGNPs were adjusted to 10 μM (CUR) in 50 μM CGNPs. The aqueous solution of CGNPs exhibited a strong absorption at 533 nm due to surface plasmon resonance (Figure 2A). CUR showed a maximum absorption at 426 nm. CGNPs did not absorb appreciably in the region near 426 nm. However, the mixed solution of CUR and CGNPs displayed absorption at both wavelengths, 426 and 533 nm, respectively. After sonication of the CUR and CGNPs, the maximum adsorption at 426 nm decreased due to the formation of CD/CUR inclusion complexes on the GNP surface. This complexation pattern was further confirmed by FTIR spectroscopy (Figure 2B). CUR exhibited absorption bands at 1605 cm^{-1} (benzene ring stretching), 1502 cm^{-1} (C═O and C═C bonds), 1435 cm^{-1} (C−H bending), 1285 cm^{-1} (C−O stretching), and 1026 cm^{-1} (C−O−C stretching). CGNPs showed absorption bands at 3430 cm^{-1} (O−H stretching), 2920 cm^{-1} (C−H stretching), 1632 cm^{-1} (O−H bending), and 1041 cm^{-1} (C−O−C stretching). In the case of CUR−CGNPs, all peaks belonging to CGNPs as well as CUR peaks were observed. These results indicate the successful formation of CD/CUR inclusion complexes on the GNP surface.

The morphology and size distribution of CGNPs and CUR−CGNPs were observed by TEM and DLS. TEM images showed that the CGNPs and CUR−CGNPs were very spherical, well-dispersed, and uniform in the range of 20−40 nm (Figure 3A,B). DLS measurements quantitatively confirmed the size distributions of CGNPs and CUR−CGNPs, resulting in 28.7 and 36.3 nm in mean size, respectively (Figure 3C). The results of TEM and DLS measurements indicated that no aggregation occurred between CGNPs after encapsulation of CUR (Figure 3).

Effects of CUR and CGNPs on the Viability of BMMs. The cell viability at different concentrations of CUR and CGNPs for BMMs was confirmed by CCK assay at different incubation time intervals (Figure 4). It was found that CUR displayed no cytotoxic effects up to a threshold concentration of 5 μM after 1, 2, and 5 days. The CGNPs exhibited no cytotoxicity after treatment with various concentrations (1, 5, 10, and 20 μM), while cytotoxicity of CUR was found at 10 μM concentration in BMMs. This result indicates that the prepared CGNPs could be useful as cytocompatible delivery vehicles.

Genotoxicity of BMMs in the Presence of CUR and CGNPs. The genotoxicity of different concentrations of CUR and CGNPs for BMMs was confirmed by comet assay at 24 h (Figure 5). As shown in Figure 5A, the CUR exhibited a slight genotoxic effect on BMMs in a dose-dependent manner. This was determined by the percentage of DNA in comet tail. On the other hand, the CGNPs showed no genotoxicity after treatment at a variety of concentrations (Figure 5B). Figure 5C shows the comet images of BMMs treated with various concentrations of CUR and CGNPs. The DNA fragmentations were found to increase with

increasing concentration of CUR, while the CGNPs exhibited no observable changes with increasing concentration.

Intracellular Uptakes of Rho-CGNPs by CLSM Analyses. To confirm the presence of GNPs in the BMMs, we prepared rhodamine B labeled CD by a previously reported method and then conjugated these to the surface of GNPs *via* Au−S bonds. [19] The fluorescence of rhodamine B is quenched on the surface of GNPs. However, as rhodamine B is cleaved by intracellular glutathione (GSH) it fluoresces by itself due to being free from quenchers. [35] Figure 6 shows the results of intracellular uptake measurements using Rho-CGNPs and cell-tracker. These measurements were confirmed by CLSM. After incubation with Rho-CGNPs, the florescence of rhodamine B was found to increase as time goes on. As shown in optical images, it was found that Rho-CGNPs effectively penetrated into the BMMs.

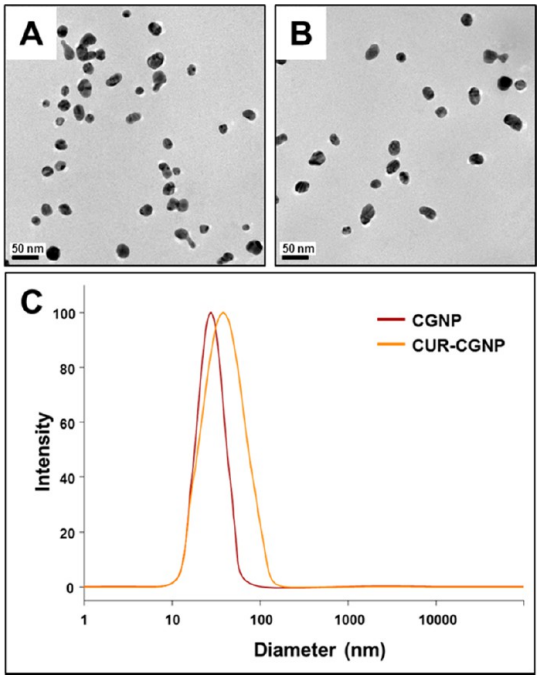

Figure 3. Structure and characterization of CGNP and CGNP-CUR: TEM images of (A) CGNP and (B) CUR−CGNP, and (C) Size distribution of CGNP and CUR−CGNP, as measured by DLS. Scale bar = 50 nm.

Supplements (CUR, CGNPs, CUR−CGNPs) Inhibit RANKL-Induced OC Formation. OC differentiation was tested by incubating BMMs in media containing osteoclastogenic cytokine RANKL (100 ng/mL) and the monocyte survival factor M-CSF (30 ng/mL), which leads to the induction of OC formation (OC induction media). This was done in the presence or absence (control) of CUR, CGNPs, and CUR−CGNPs. Before testing the effects of CUR and CGNPs on OC differentiation, the cytotoxicity of these supplements was examined in BMMs by a CCK-8 kit (Figure 4). It was found that CUR showed some cytotoxicity toward BMMs when used at 10 μM concentration. Therefore, CUR was used at concentrations below 5 μM in order to compare the inhibition effect of osteoclastogenesis in the absence of cytotoxicity. The effect of supplements (CUR and CGNPs) on OC differentiation was confirmed by TRAP staining (Figure 7). Cells were stained for the OC marker TRAP (purple cells) and photographed under light microscopy, and the number of $TRAP^+$ MNCs was counted. As shown in Figure 7A,B, the largest number of $TRAP^+$ MNCs at 5 days of culture was detected with the OC induction media alone control group. On the other hand, it was visually observed that the stained $TRAP^+$ MNCs decreased in a dose-dependent manner relative to CUR and CGNPs. CUR inhibited the formation of $TRAP^+$ MNCs from 197.6 ± 11.2 (control) to 144.3 ± 10.7, 116.3 ± 11.8, and 44.3 ± 6.1 (73.0%, 58.8%, and 22.4%) at 0.5, 1, and 5 μM, respectively. Additionally, CGNPs inhibited the formation of $TRAP^+$ MNCs from 198.3 ± 6.5 (control) to 163.6 ± 11.1, 71.6 ± 11.0, 26.0 ± 3.6, and 8.0 ± 2.6 (82.5%, 36.1%, 13.1%, and 4.0%) at 1, 5, 10, and 20 μM, respectively (Figure 7C). The highest dose of CUR and CGNPs displayed the highest inhibitory effects toward OC differentiation of BMMs.

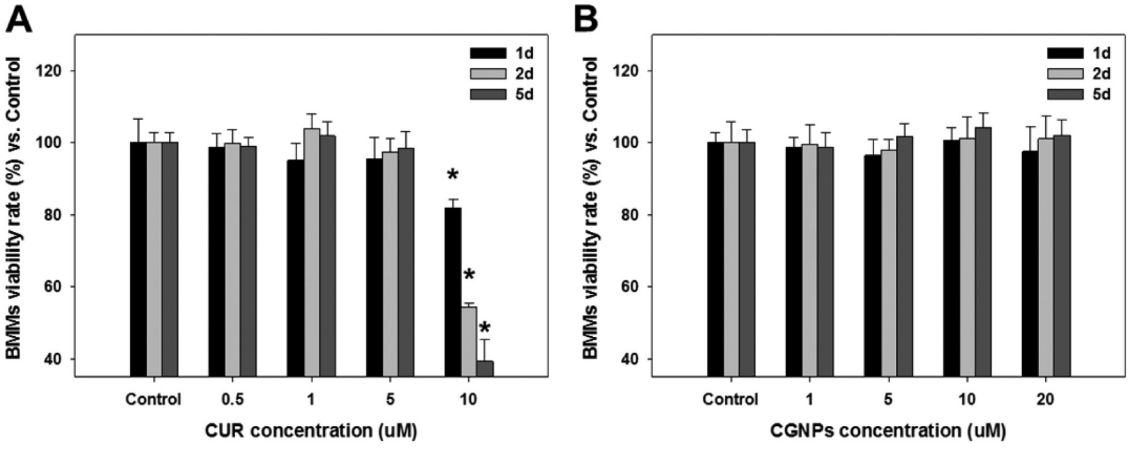

Figure 4. Viability of BMMs in the presence of (A) CUR and (B) CGNPs at different concentrations. Results are mean ± SD of triplicate experiments: *$p < 0.01$, significant difference as compared with control.

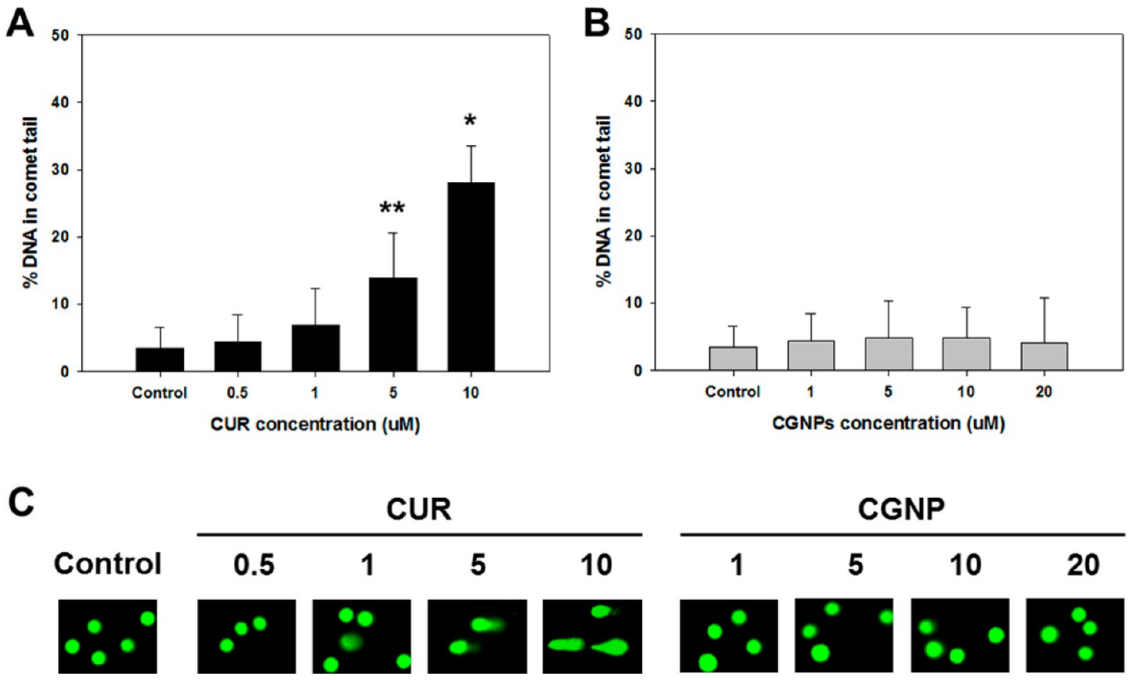

Figure 5. Genotoxicity of BMMs in the presence of CUR and CGNPs at 24 h, measured by the comet assay: DNA fragmentation (% DNA in comet tail, mean ± SD) in the presence of (A) CUR and (B) CGNPs and (C) representative comet images from treatment with CUR and CGNPs at different concentrations. Results are mean ± SD of triplicate experiments: *$p < 0.01$, **$p < 0.05$, significant differences as compared with control.

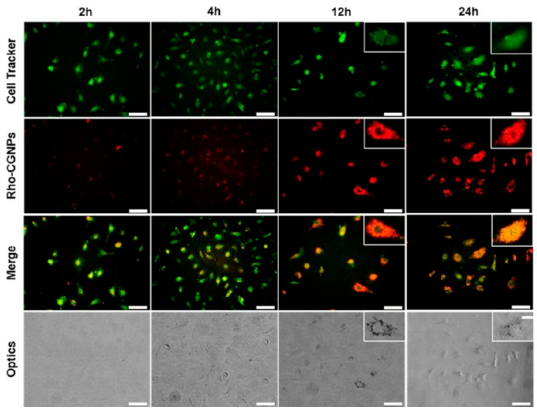

Figure 6. Intracellular uptake images of BMMs treated with Rho-CGNPs and cell tracker, as confirmed by CLSM. The fluorescence of Rho-CGNPs was increased as time goes on after intracellular uptake. Scale bar = 50 μm.

To verify the effect of CUR–CGNPs as compared with CUR and CGNPs, BMMs were cultured in the presence or absence of CUR (1 and 5 μM), CGNPs (5 and 10 μM), and CUR–CGNPs (1/5 and 1/10 μM). BMMs differentiated efficiently into TRAP$^+$ MNCs in the absence of supplements (201 ± 12.0), while the formation of TRAP$^+$ MNCs was decreased in a dose-dependent manner in the presence of CUR, CGNPs, and CUR–CGNPs (Figure 8A). The average counted values of TRAP$^+$ MNCs treated with 1 μM CUR, 5 μM CUR, 5 μM CGNPs, 10 μM CGNPs, 1/5 μM CUR–CGNPs, and 1/10 μM CUR–CGNPs were 111.3 ± 10.6 (55.2%), 41.0 ± 13.1 (20.3%) 78.6 ± 10.2 (39%), 30.0 ± 4.6 (14.8%), 42.3 ± 9.4 (20.9%), and 9.6 ± 3.5 (4.8%), respectively (Figure 8B). Moreover, 1/10 μM CUR–CGNPs displayed the highest reduction of TRAP$^+$ MNCs. This indicates that the CGNPs can effectively deliver CUR and inhibit the OC differentiation of BMMs. Also, this combination displays a synergistic effect on the inhibition of OC formation.

Supplements (CUR, CGNPs, CUR–CGNPs) Inhibit Actin Ring formation. RANKL is known to accelerate bone resorption as this is the main function of mature OC. OC displays an actin ring which is a unique cytoskeletal structure that allows them to resorb bone. The actin ring formation of BMMs incubated in OC induction media with or without CUR, CGNPs, and CUR–CGNPs was confirmed by immunofluorescence analysis. It was found that RANKL stimulated actin ring formation, while supplements (CUR, CGNPs, and CUR–CGNPs) reduced actin ring formation (Figure 9). Moreover, CUR–CGNPs showed almost no actin ring formation as compared to the other groups. From these results, we suggest that the CUR–CGNPS can be useful as therapeutic agents for osteoporosis.

Supplements (CUR, CGNPs, CUR–CGNPs) Lead to the Down Regulation of Osteoclastogenic Genes and Transcriptional Regulators. To investigate the effect of supplements on the expression of OC-specific genes in RANKL-treated BMMs, the mRNA expressions of c-Fos, NFATc1, TRAP, and OSCAR were determined by real-time PCR (Figure 10). Control, with or without RANKL, was used as positive and negative controls, respectively. The results were normalized to GAPDH expression. The c-Fos and NFATc1 have been shown to be

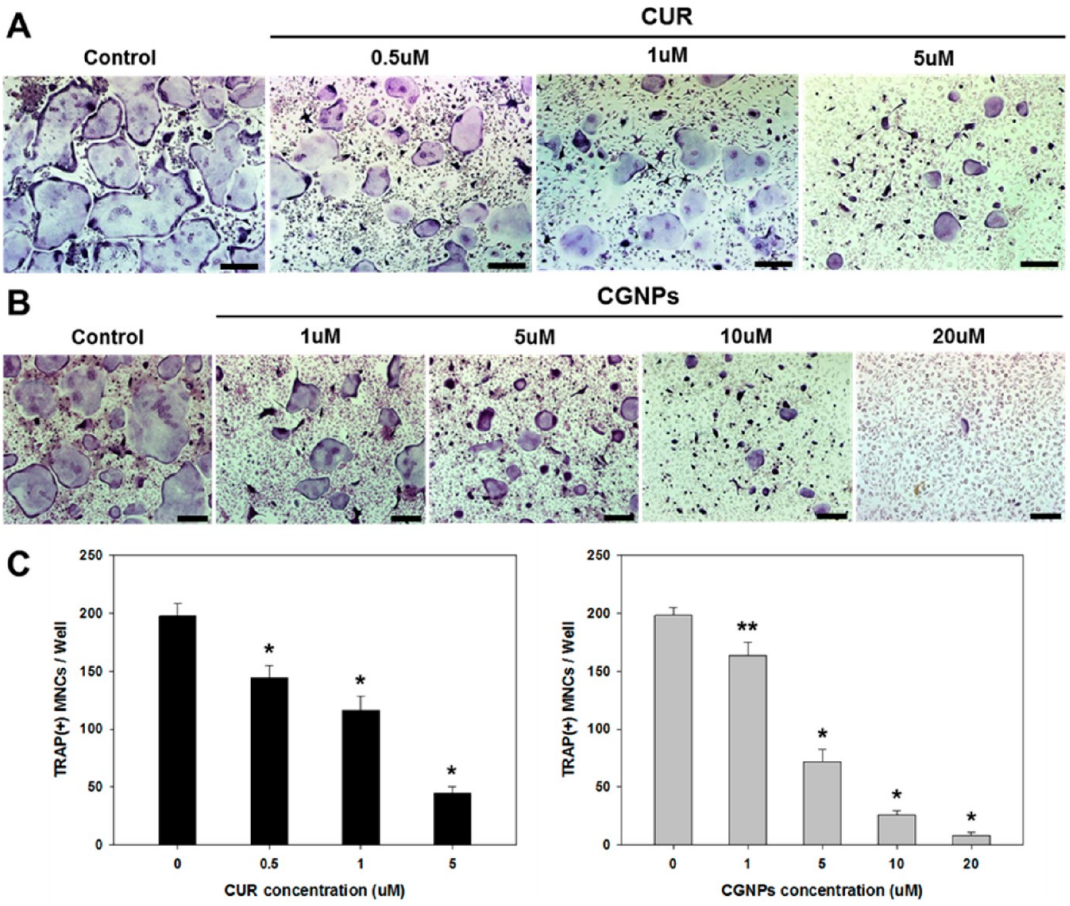

Figure 7. TRAP assay after treatment with CUR and CGNPs. TRAP+ MNCs decreased in a dose-dependent manner relative to CUR and CGNPs. Scale bar = 200 μm. Results are mean ± SD of triplicate experiments: *p < 0.01, **p < 0.05, significant difference as compared with the control.

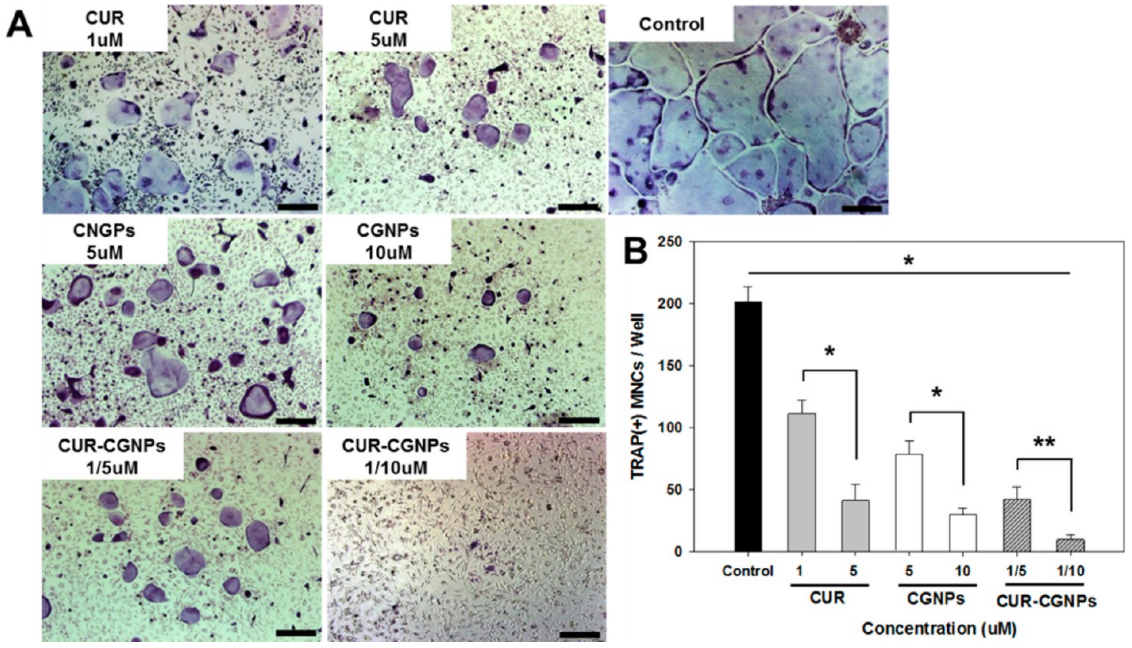

Figure 8. TRAP assay after treatment with CUR, CGNPs, and CUR−CGNPs. The formation of TRAP+ MNCs were decreased in a dose-dependent manner in the presence of CUR, CGNPs, and CUR−CGNPs. Scale bar = 200 μm. Results are mean ± SD of triplicate experiments: *p < 0.01, **p < 0.05, significant difference as compared with the control and each other.

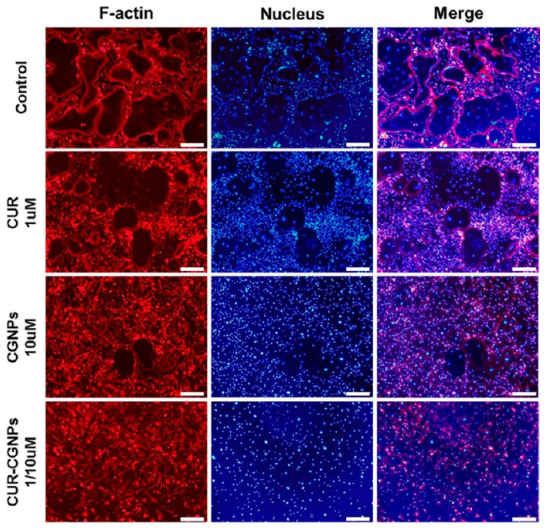

Figure 9. Effect of CUR, CGNPs, and CUR−CGNPs on RANKL-induced actin ring formation in BMMs. The CUR−CGNPs showed almost no actin ring formation as compared to the other groups. Scale bar = 200 μm.

up-regulated after RANKL stimulation and are the most important OC-specific transcription factors involved in OC differentiation.[36,37] The stimulation of BMMs in the presence of RANKL induced high mRNA expressions of both c-Fos and NFATc1. After treatment with supplements, the expression levels of these markers were significantly decreased in the order of CUR, CGNPs, and CUR−CGNPs (Figure 10A and B). Among these supplements, CUR−CGNPs showed the lowest mRNA expression of c-Fos and NFATc1. All supplements significantly inhibited the induction of TRAP and OSCAR genes, which are enhanced by c-Fos and NFATc1 (Figure 10C,D). The mRNA expressions of TRAP and OSCAR were significantly decreased in the presence of CUR−CGNPs, and this result correlated well with the prior results for $TRAP^+$ MNCs generation. Overall, all supplements led to the down-regulation of osteoclastogenic genes (TRAP and OSCAR) and transcriptional regulators (c-Fos and NFATc1) in the order of CUR, CGNPs, and CUR−CGNPs. In particular, CUR−CGNPs showed the lowest mRNA expressions for all markers.

Effects of CGNPs and CUR−CGNPs on RANKL-Induced Signaling Pathways. To investigate the inhibitory effects of CUR-GNPS on OC differentiation, the biological mechanisms of RANKL-induced signaling pathways were confirmed by Western blotting (Figure 11). BMMs were stimulated with RANKL in the presence or absence of CGNPs and CUR−CGNPs. The activation/inactivation levels of MAPKs (p38, ERK, and JNK) and IκBα, which regulate the process of OC differentiation,[38,39] were measured at predetermined time points. Whole protein expression levels were confirmed by specific phosphor-antibodies which were the active forms of the respective molecules. The results showed that the CGNPs exhibited an increase in the p38 phosphorylation level after 30 min, but the CUR reduced p38 activation. Therefore, the CUR−CGNPs exhibited no substantial enhancement of p38 activation as compared with RANKL only. These results indicate that the p38 signaling pathway was up-regulated by CGNPs and down-regulated by CUR. The expression levels of p-ERK, p-JNK, and p-IκBα were slightly decreased in either groups of CGNPs and CUR. Therefore, CUR−CGNPs lead to more substantially decreased expression levels of p-ERK, p-JNK, and p-IκBα than CGNPs and CUR alone. This indicates that both CGNPS and CUR inhibit these signaling pathways by interaction with BMMs. Additionally, we confirmed the protein expression levels of another RANKL-induced signal pathway, Akt, which is an important protein for the in inhibition of cell death.[40,41] The expression level of p-Akt was slightly increased in the presence of CGNPs, and decreased in CUR. This indicates that the Akt signaling pathway is up-regulated by CGNPs and down-regulated by CUR.

Supplements (CUR, CGNPs, CUR−CGNPs) Prevented Bone Loss *in Vivo*. As all supplements inhibited osteoclast differentiation *in vitro*, we examined the effect of CGNPs (dose: 500 μM CGNPs), CUR (dose: 50 μM CUR), and CUR−CGNPs (dose: 50/500 μM CUR−CGNPs) on the prevention of ovariectomy (OVX)-induced bone loss. For all experimental periods, no significant change was observed in body weight of all groups (Figure S3, Supporting Information). All groups, treated with or without supplements, were analyzed by soft X-ray (radiographic analysis). It was visually observed that the bone densities of all experimental groups were enhanced as compared with that of OVX group during 9 weeks (Figure 12A). Also, all experimental groups treated with supplements had a statistically significant increase in relative bone densities (Figure 12B). Figure 13A shows the hematoxylin and eosin (H&E) staining images of the femoral bone. It was visually observed that all ovariectomized groups had a higher amount of adipose tissue as compared to the sham group. Among all of these groups, the trabecular bone is much more prominent in CGNPs and CUR−CGNPs groups. In addition, the relative trabecular bone dimensions in femur tissue showed that all experimental groups were higher than nontreated OVX groups. CUR−CGNPs had the highest trabecular bone dimensions for all tested groups (Figure 13B). μCT analysis was performed to quantify the bone density. The structural parameters of trabecular bone for bone volume/tissue volume (BV/TV), bone mineral density (BDM), BV, trabecular number (Tb.N), trabecular thickness (Tb.Th), and trabecular separation (Tb.Sp) are illustrated in Figure 14 and Figure S5 (Supporting Information). As shown in Figure 14A, the thickness of trabecular bone was significantly decreased after OVX. After treatment with supplements, the femoral bone densities were visually increased in all groups as compared with OVX control. A significant increase of

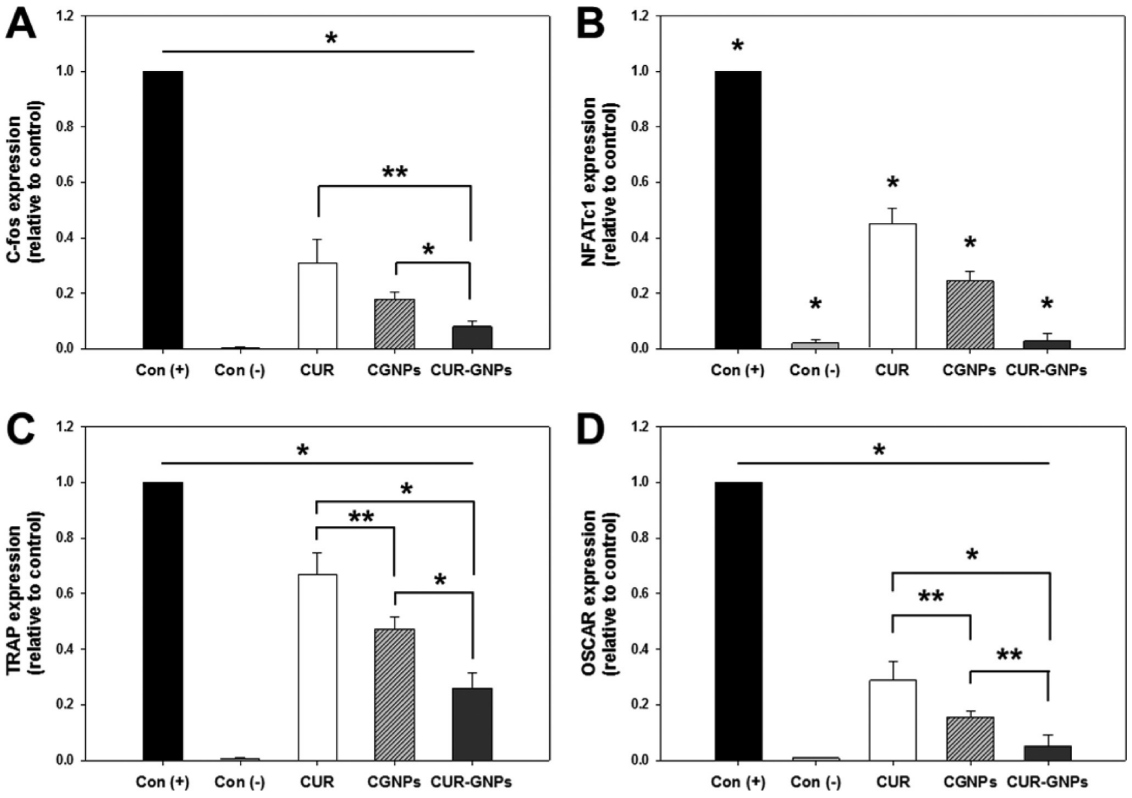

Figure 10. Gene expression of (A) c-Fos, (B) NFATc1, (C) TRAP, and (D) OSCAR in the presence of CUR (1 μM), CGNPs (10 μM), and CUR−CGNPs (1/10 μM). Results are mean ± SD of triplicate experiments: *$p < 0.01$, **$p < 0.05$, significant difference as compared with each other. All groups were treated with RANKL, and control without RANKL [Con(−)] was used as negative control.

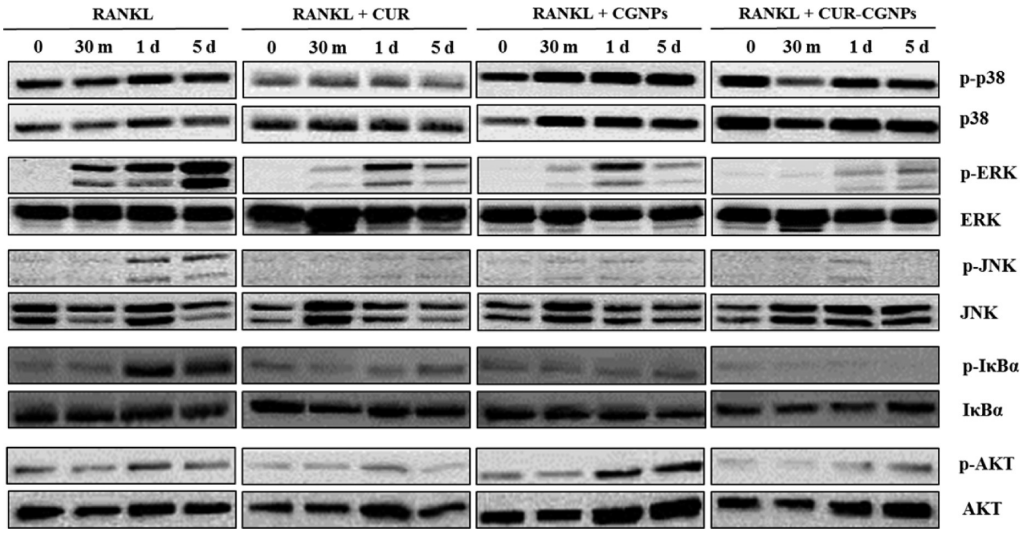

Figure 11. Protein expression of phosphorated p38, ERK, JNK, IκBα, and Akt in the presence of CGNPs (10 μM) and CUR−CGNPs (1/10 μM). The blot is a representative image of three independent experiments.

bone thickness was identified in the bone treated with CGNPs and CUR−CGNPs. In comparison with OVX group, CUR, CGNPs, and CUR−CGNPs groups exhibited 0.004%, 1.417%, and 1.609% greater BV/TV than OVX, respectively (Figure 14B). Also, it was found that the BMD values of CGNPs and CUR−CGNPs were significantly higher than the OVX group (Figure 14C). Furthermore, CUR−CGNPs exhibited the most improved bone density as compared to the other groups, and showed a similar values with Sham in all structural parameters of trabecular bone (Figure S5, Supporting Information).

DISCUSSION

Bone is continuously remodeled through the removal of old or damaged bone by OCs and the subsequent replacement of new bone by osteoblasts. The processes of bone formation and resorption are well regulated and balanced by several factors. An

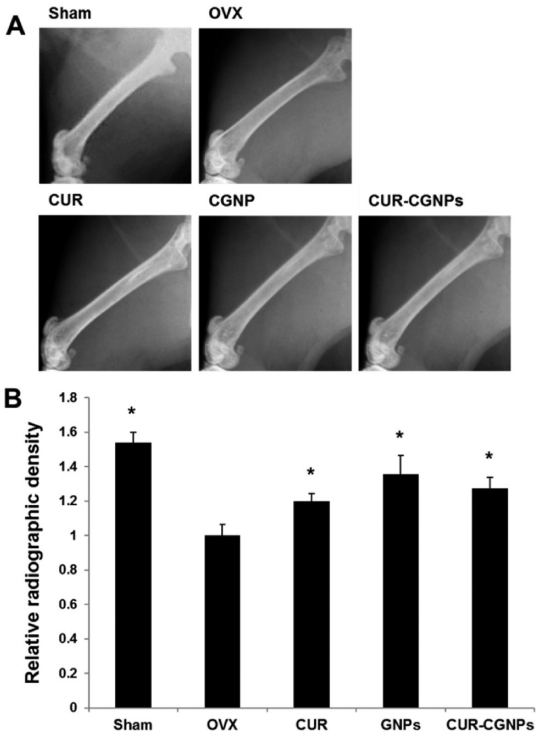

Figure 12. Radiographic analysis of bone tissue in mice. (A) Radiographic images of left femur and (B) average of relative bone density value in all experimental groups. Relative bone densities of all experimental groups were higher than that of OVX group during 9 weeks, and the difference was statistically significant. For analysis, left and right femurs were averaged for each mouse. n = 5 per group: *p < 0.01, significant difference as compared with OVX.

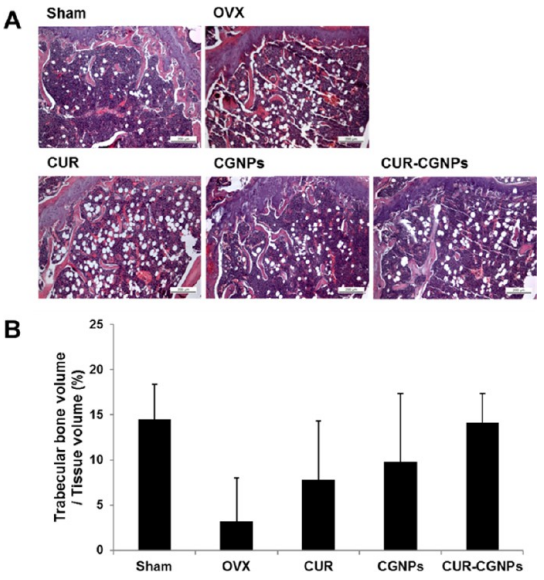

Figure 13. Histological analysis of femora from all experimental groups (n = 5 per group). (A) H&E staining of femur bone. Scale bar = 200 μm. Histology of bone in the all-experimental groups shows all ovariectomized groups had a higher amount of adipose tissue than sham group. The trabecular bone is much more prominent in CGNPs and CUR−CGNPs groups. (B) Relative trabecular bone dimension shows all experimental groups were higher than non-treated, OVX group. CGNPs and CUR−CGNPs groups had much more trabecular bone dimension than the other groups but the difference was not significant (p > 0.05).

imbalance between these processes leads to bone diseases such as osteoporosis and rheumatoid arthritis. Osteoporosis is a devastating disease that leads to an increased risk of bone fracture by lowering bone mineral density. This disease frequently occurs in older people, especially women.[14,15] To treat this, bisphosphonate molecules are widely used to prevent the loss of bone mass and bone fracture.[42,43] However, when bisphosphonates are administered for an extended period, serious side effects occur, such as osteonecrosis of the jaws.[44] To solve this problem, there has been a great deal of recent research in developing new generations of agents for preventing and treating osteoporosis. A number of researchers have reported that various inorganic NPs can inhibit OCs formation. OCs are involved mainly in bone resorption, and these inorganic materials, such as gold, platinum, and silica-based NPs, substantially suppress osteoclastogenesis.[11−13] Among previously researched inorganic-based NPs, GNPs have been shown to be the most effective material for treating bone diseases because of their potential use not only for inhibition of OC differentiation but also for stimulation of osteoblast formation.[4−6,11] Also, GNPs exhibited no *in vivo* toxicity. Previous reports have shown that 30 nm GNPs did not cause any significant damage to internal organs, despite their accumulation in the liver, spleen, and kidney after intraperitoneal injection.[45,46]

Based on this information, we prepared a novel agent using 30 nm GNPs for the inhibition of OC formation. To enhance the therapeutic effects of this agent for the treatment of osteoporosis, CD-modified GNPs were prepared and used as carriers of CUR, an osteoporosis drug. CUR is known to be a powerful antioxidant and suppress RANKL-mediated ROS generation. Previously, we reported that CUR suppressed ROS-induced IκBα signaling pathways and thereafter inhibits signal pathways for osteoclastogenesis.[31] Also, CUR can form inclusion complex interactions with CD, which improves the water solubility of CUR.[23,26−28,32−34] Therefore, CUR was loaded onto the surface of CGNPs to enhance the inhibitory effects of the system toward osteoclastogenesis. The formation of CGNPs and CUR−CGNPs was confirmed and characterized by UV−vis spectroscopy, TEM, and DLS (Figure 2 and 3). It was found that CGNPs prepared by our group displayed no cytotoxicity and genotoxicity up to 20 μM (Figures 4 and 5). This result might indicate that the prepared CGNPs can be useful as a cytocompatible agent, unlike CUR alone which is cytotoxic at high concentrations.

Previous studies have shown that CUR inhibits RANKL-induced IκBα signaling pathways through the suppression of p-IκBα.[30,31] RANKL, which is a key factor to control function and survival of mature osteoclasts, induces multiple signaling pathways. This includes not

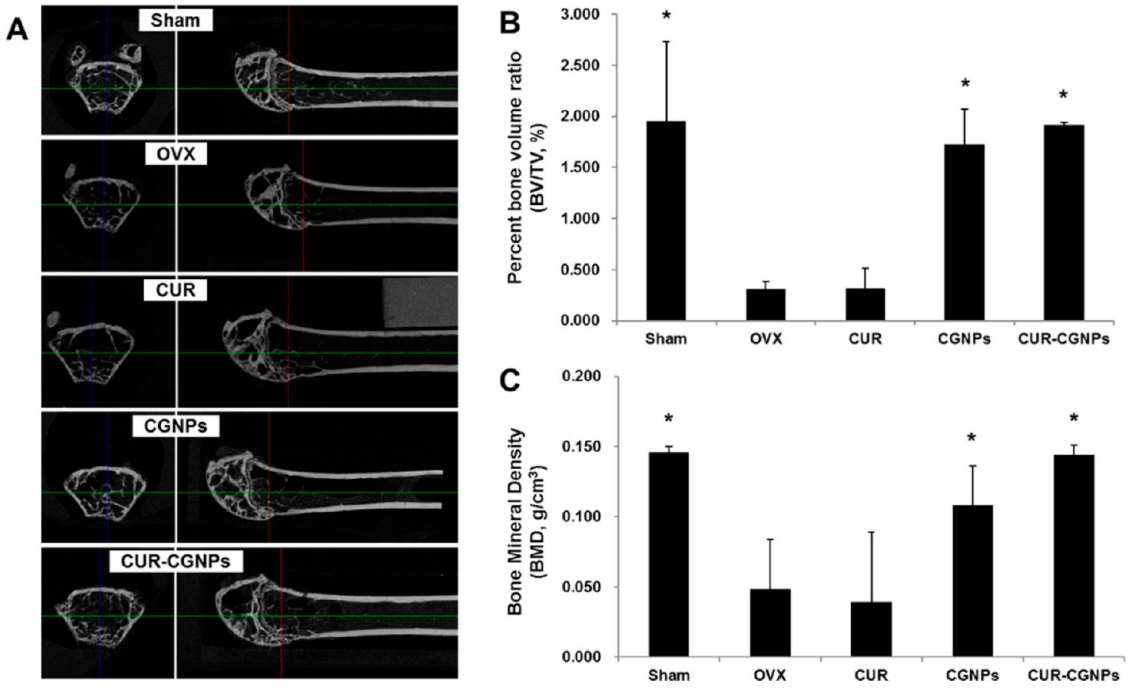

Figure 14. μCT analysis of bone tissue in mice. (A) 3D images of trabecular bone measured by μCT. Representative images of Sham, OVX, CUR, CGNPs and CUR−CGNPs from top to bottom. Sham group was used as the positive control. Average value of (B) percent bone volume ratio and (C) bone mineral density in all experimental groups. Average values of Sham, CGNPs, and CUR−CGNPs were higher than that of OVX group during 9 weeks, and the difference was statistically significant. n = 5 per group: *p < 0.01, significant difference compared with OVX.

only IκBα but also others such as JNK, P38, and ERK. Although Sul *et al.* described that GNPs are involved in OC differentiation of BMMs through NF-kB signaling,[11] the biological mechanisms have not been studied in detail as to how gold nanoparticles can affect OC differentiation of BMMs through multiple signaling pathways such as IκBα, JNK, P38, and ERK. Therefore, we confirmed the effect of CUR, CGNPs, and CUR−CGNPs on inhibition of OC differentiation by using BMMs in the presence of RANKL and M-CSF. The *in vitro* results showed that all supplements of CUR, CGNPs, and CUR−CGNPs lead to a decrease in $TRAP^+$ MNCs formation. These also lead to a down-regulation of gene expressions which are associated with the RANKL-induced OC differentiation pathway (Figures 7, 8, and 10). This is with the exception of p38 which was up-regulated in the presence of CGNPs. Of all the tested supplements, CUR−CGNPs showed the lowest value of $TRAP^+$ MNCs formation and mRNA expressions. Also, CUR−CGNPs substantially inhibited RANKL-induced actin ring formation, which is an essential morphological characteristic of OC that allows them to carry out their resorption function (Figure 9). To confirm the activation/inactivation levels of key proteins involved in OC differentiation pathways, such as p38, ERK, JNK, and IκBα, Western blotting was used at predefined time points. The results clearly showed that the CUR−CGNPs exhibited no substantial enhancement in p38 but did decrease expression levels of p-ERK, p-JNK, p-IκBα, and Akt as compared with RANKL only (Figure 11). Furthermore, our biofunctional GNPs, surface-functionalized with CD/CUR inclusion complex, have successfully prevented bone loss *in vivo*, as evaluated by the OVX-induced osteoporosis model (Figures 12−14). There was no remarkable difference in the relative bone densities between all experimental groups treated with supplements (Figure 12). However, we identified that more trabecular bone tissue appeared in CGNPs and CUR−CGNPs than in the other experimental groups, and CUR−CGNPs had the highest trabecular bone dimensions for all tested groups (Figure 13). In addition, the results of μCT indicated that the average value of CGNPs and CUR−CGNPs were higher than that of OVX groups, and the difference was significant (Figure 14). In addition, CUR−CGNPs exhibited the most improved bone density of all tested groups. Although there was no remarkable difference between CGNPs and CUR−CGNPs, almost all of the results consistently showed that CUR−CGNPs is the most improved bone density as compared with all tested groups.

On the basis of the above findings, a schematic diagram was proposed to describe the inhibition of OC differentiation of BMMs by CUR−CGNPs (Figure 15). CUR−CGNPs first interact with the membrane of BMMs and effectively release CUR into the intracellular cytoplasm. The suppression of the RANKL-induced signaling pathway leads to a down-regulation of the OC-specific transcription factors and osteoclastogenic genes involved in OC differentiation. Therefore, these

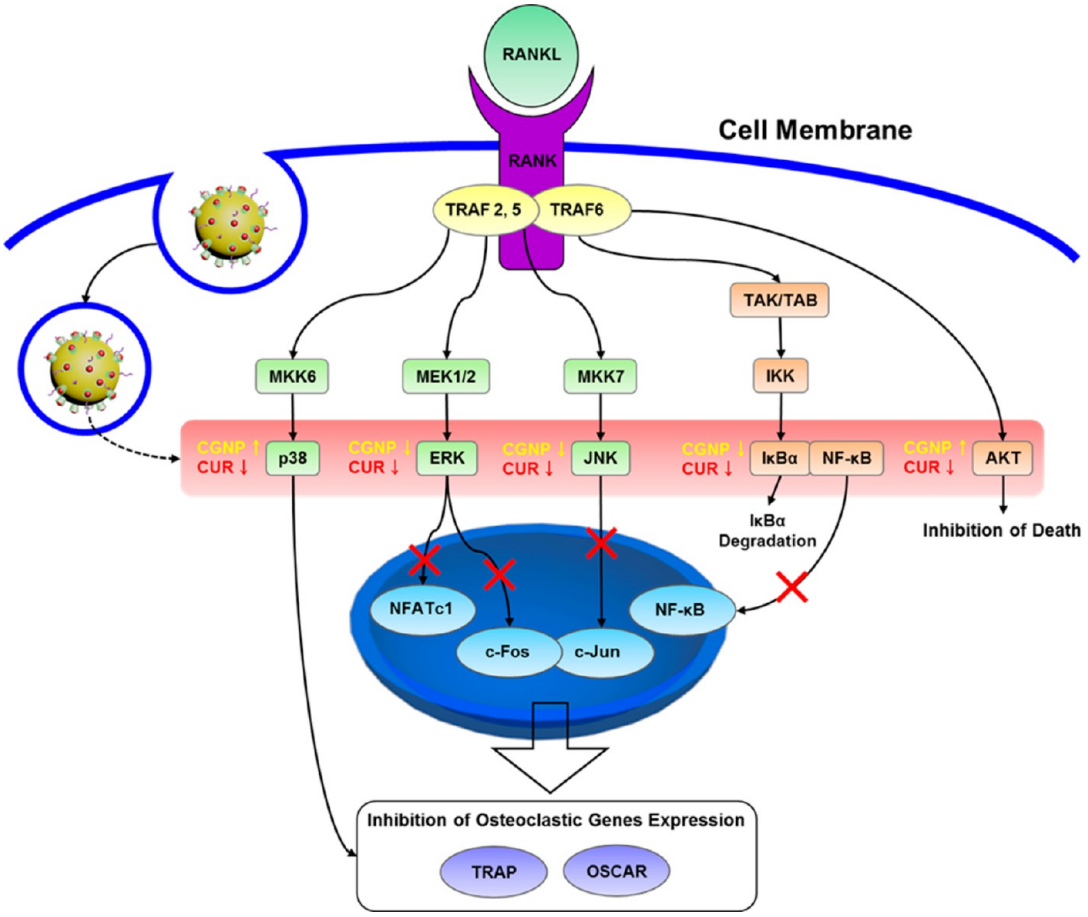

Figure 15. Biological mechanism leading to inhibition of OC differentiation of BMMs by CUR−CGNPs through RANKL-induced signaling pathways.

results indicate that CUR−CGNPs can act as effective nanocarriers for delivering CUR, and serve as a mechanical stearic hindrance which deactivates the RANK-induced signaling pathway in BMMs. This subsequently leads to a down-regulation of OC differentiation. The *in vivo* application of functionalized GNPs significantly prevented bone resorption and improved bone metabolism. This *in vivo* result is especially remarkable. Previous researchers have confirmed the inhibition of osteoclast differentiation under *in vitro* conditions but not *in vivo*. The results of *in vitro* assays may not always be the same as that of *in vivo*. Therefore, *in vivo* studies are important to confirm the preventability of bone resorption by GNPs.

CONCLUSION

In this study, we designed and prepared a novel therapeutic agent for preventing and treating osteoporosis. This was composed of GNP as a core, CD as a drug pocket, and CUR as an osteoporosis drug. Intracellular uptake analysis showed that CGNPs can effectively be uptaken into the cell and locate into the intracellular compartment. The CUR−CGNPs inhibited the OC differentiation of BMMs through suppression of the RANKL-induced signaling pathway. The biofunctional GNPs may consequently have significant potential applications for use as therapeutic agents in treating osteoporosis and other bone diseases, such as rheumatoid arthritis or metastasis associated with bone loss. Furthermore, to our knowledge, this study is the first example that confirms the effect of GNPs for preventing osteoporosis in an *in vivo* model. Our findings suggest that CUR−CGNPs can be useful as therapeutic agents for treating bone diseases associated with excessive bone resorption.

MATERIALS AND METHODS

Materials and Equipment. CD surface-functionalized GNPs (CGNPs) and rhodamine B linked CD surface-functionalized GNPs (Rho-CGNPs) were prepared as previously reported.[19] CUR and Leukocyte Acid Phosphatase Assay kit were purchased from Sigma-Aldrich (St. Louis, MO). RANKL and macrophage-colony stimulating factor (M-CSF) were obtained from Peprotech (Rocky Hill, NJ). α-Minimum essential medium (α-MEM), fetal bovine serum (FBS), Dulbecco's phosphate-buffered saline (DPBS), trypsin−EDTA, and penicillin−streptomycin (PS) were

purchased from GIBCO BRL (Invitrogen Co., Carlsbad, CA). Cell tracker green was purchased from Molecular Probes (Invitrogen Co., USA) All antibodies for p38, phospho-p38 (Thr180/Tyr182), extracellular signal-regulated kinase (ERK), phospho-ERK, c-Jun N-terminal kinase (JNK), phospho-JNK, nuclear factor of kappa light polypeptide gene enhancer in B-cells inhibitor, alpha (IκBα), phosphor-IκBα, Akt, and phosphor-Akt were purchased from Cell Signaling Technology (Beverly, MA). All reagents were used as received without further purification. Transmission electron microscopy (TEM) observations were carried out using an H-7100 (Hitachi, Japan). Dynamic light scattering (DLS) measurements were carried out using a 90 PLUS (Brookhaven, Holtsville, NY). Ultraviolet/vis (UV/vis) absorbance was measured using a UV-1650PC spectrophotometer (Shimadzu, Japan). Attenuated total reflectance-Fourier transform infrared (ATR-FTIR) measurements were carried out using a TENSOR 37 (Bruker, Billerica, MA).

Preparation of GNPs Covered with CD/CUR Inclusion Complex (CUR−CGNP). To load CUR onto the surface of GNPs, 10 μL of 2.5 mM CUR, dissolved in dimethyl sulfoxide (DMSO), was added to 50 μM CGNPs solution (1 mL), and the resulting solution was then sonicated for 5 min. After centrifugation, the precipitate was washed three times with distilled water. The loading efficiency of CUR into CGNPs was measured by using a UV/vis spectrophotometer at a detection wavelength of 426 nm.

Cell Culture. Primary cultured BMMs were used to study cell cytotoxicity and OC differentiation. For generation of bone marrow-derived osteoclasts, monocytes were isolated from the tibiae of ICR 6 week mice as previously described.[47] Cells were seeded on 100 mm plates (1.5×10^6/well) and cultured in the presence of 30 ng/mL M-CSF for 72 h. Cells at this stage were considered M-CSF-dependent BMMs and used as preosteoclasts. The cells were cultured in α-MEM containing 10% FBS and 1% PS in a humidified 5% CO^2 atmosphere. Induction of differentiation to OC was achieved by culturing the cells in a media containing RANKL (100 ng/mL) and M-CSF (30 ng/mL) with or without varying doses of test supplements (CUR, CGNP, and CUR−CGNP). The complete culture medium containing different supplements was changed every 3 days. For biological experiments and analyses, the cells were harvested, collected by centrifugation at 1000 rpm for 5 min, and then seeded in well plates before *in vitro* biological evaluation.

Cell Viability Assay. The cell viability of the different supplements was evaluated by using by using a cell counting kit (CCK-8, Dojindo Molecular Technologies Inc., Japan) assay. After seeding the cells, adhered and proliferated cells were measured at 24 and 48 h. At predetermined time intervals, cells were washed with DPBS, a fresh medium containing CCK-8 (300 μL of 0.1 mL/ml) was added, and then the cells were incubated for 2 h. After incubation, the intensity was measured by a microplate reader (BioRad, USA) at a wavelength of 450 nm.

Comet Assay. The comet assay was carried out according to Javeri *et al.*[48] using reagents provided in a kit purchased from Trevigen, Gaithersburg, MD. In brief, cell suspension at 1×10^5 cells/ml was diluted with low melting point agarose at a ratio of 1:10 (v/v) and immediately spread onto CometSlide. The slides were allowed to solidify at 4 °C for 10 min and immersed in 4 °C lysis solution for 1 h. After lysis, DNA on the slides were separated by electrophoresis and visualized by SYBR Green 1 staining solution. Images were captured using an Olympus fluorescence microscope (Tokyo, Japan) and analyzed using Comet Assay IV software (http://www.scorecomets.com). DNA damage was quantified as percentage of DNA in tail (% tail DNA).

Intracellular Uptakes of Rho-CGNPs As Determined by Confocal Laser Scanning Microscopy (CLSM) Analyses. BMMs (2×10^4 cells/per well) were seeded in 48 well-culture plates and incubated overnight in preparation for CLSM analysis. After incubation, the media was exchanged for fresh media containing Rho-CGNPs and cell tracker and then incubated for 2, 4, 12, and 24 h, respectively. After the media were removed, the cells were washed with fresh DPBS and fixed with 3.7% formaldehyde. Intracellular uptake of Rho-CGNPs was observed by CLSM (Eclipse E600W, Nikon, Tokyo, Japan). The obtained images were assayed by using Nikon EZ-C1 software.

Tartrate-Resistant Acid Phosphatase (TRAP) Assay. BMMs (2×10^4 cells/per well) were seeded in 48 well-culture plates and incubated with complete culture medium containing different supplements. TRAP-positive multinuclear cells ($TRAP^+$ MNCs) were observed after 5 days. Cells were fixed by soaking in 3.7% formaldehyde for 15 min and were then placed in 0.1% triton X-100 for 10 min. Cells were washed three times with DPBS, and then incubated for 30 min at 37 °C in the dark using the Leukocyte Acid Phosphatase Assay kit following the manufacturer's instructions. After staining, $TRAP^+$ MNCs containing three or more nuclei were considered to be OCs and scored under a light microscope.

Actin Ring Formation Assay. BMMs (2×10^4 cells/per well) were seeded in 48 well-culture plates in the presence of complete culture medium for 5 days. Subsequently, the cells were fixed in 3.7% formaldehyde for 20 min. After three washings with DPBS, the cells were stained with rhodamine-conjugated phalloidin and 4′,6-diamidino-2-phenylindole (DAPI) for 30 min and washed with DPBS three times again. The actin ring formation of each sample was observed by confocal laser scanning microscopy (CLSM, Eclipse E600W, Nikon, Tokyo, Japan).

Quantitative Real-Time Polymerase Chain Reaction (Real-Time PCR). The total RNA of the BMMs (a density of 2×10^4 cells) cultured on a 48 well-culture plate was isolated by using an RNeasy Plus Mini Kit (Qiagen, CA) according to manufacturer's instructions. A sum of 1 μg of total RNA was transcribed into cDNA with AccuPower CycleScript RT Premix (Bioneer, Daejeon, Republic of Korea). The primers of the measured mRNA genes were as follows: TRAP, 5′-CTG GAG TGC ACG ATG CCA GCG ACA-3′ (sense) and 5′-TCC GTG CTC GGC GAT GGA CCA GA-3′ (antisense); osteoclast-associated receptor (OSCAR), 5′-CTG CTG GTA ACG GAT CAG CTC CCC AGA-3′ (sense) and 5′-CCA AGG AGC CAG AAC CTT CGA AAC T-3′ (antisense); c-Fos, 5′-CTG GTG CAG CCC ACT CTG GTC-3′ (sense) and 5′-CTT TCA GCA GAT TGG CAA TCT C-3′ (antisense); NFATc1, 5′-CTC GAA AGA CAG CAC TGG AGC AT-3′ (sense) and 5′-CGG CTG CCT TCC GTC TCA TAG-3′ (antisense); and glyceraldehyde 3-phosphate dehydrogenase (GAPDH), 5′- CAT GGC CTT CCG TGT TCC TAC CC-3′ (sense) and 5′-CCT CAG TGT AGC CCA AGA TGC CCT-3′ (antisense). Real-time PCR was analyzed by using iQ SYBR Green supermix (Bio-Rad, Hercules, CA). Threshold cycle values were calculated by using a comparative cycle threshold method. The fold change of control (treatment with RANKL and M-CSF) at 5 days of culture was set at 1-fold and the ratio of the normalized fold change was calculated. The real-time PCR amplifications were carried out for 10 s at 95 °C, 30 s at 57−66 °C, and 30 s at 72 °C for 45 cycles after the initial denaturation step of 10 min at 95 °C. All results were normalized by GAPDH.

Western Blot. BMMs were lysed by the addition of cold RIPA lysis buffer containing 0.5 M Tris-HCl, pH 7.4, 1.5 M NaCl, 2.5% deoxycholic acid, 10% NP-40, and 10 mM EDTA along with protease and phosphatase inhibitors. The cell lysates were incubated in an ice box for 30 min and then centrifuged at 13000 rpm for 10 min. The concentration of protein was measured using a microplate spectrophotometer (Benchmark Plus, BIO-RAD, Japan) at a wavelength of 595 nm. An equal quantity of protein (40ug) was subjected to SDS-PAGE and transferred to a nitrocellulose transfer membrane (Protran, Whatman, Germany). After blocking with 5% skim milk, the membrane was probed with phosphorylated-forms of p38 (Thr180/Tyr182), ERK, JNK, IκBα, and Akt followed by incubation with an appropriate secondary antibody conjugated to horseradish peroxidase. The same membranes were then stripped and reprobed with the total forms of p38, ERK, JNK, IκBα, and Akt. Signals were detected using a ChemiDoc XRS System (Bio-Rad, Hercules, CA).

Animal Test. Female 10-week-old C57Bl/6 mice (n = 30) weighing an average of 20 g were purchased from Orient Bio (Seongnam, Korea). All animal experiments were approved by the Institutional Animal Care and Use Committee of Konkuk University (KU13118). OVX or sham operation was performed at the age of 12 weeks. OVX animals had their ovaries removed, and sham-operated animals had their ovaries exposed but not removed. The OVX mice were randomized and divided into experimental groups (n = 5 per group) as follows. The experimental groups included OVX (untreated), CGNPs (dose: 500 μM

CGNPs), CUR (dose: 50 μM CUR), and CUR−CGNPs (dose: 50/500 μM CUR−CGNPs). Injectable solutions were prepared every day as a solution of each treatment dose in physiological saline. The experimental groups were subjected to intragastric injection of each solution (0.5 mL per day). After 9 weeks of treatment, radiographic analysis of the femora was performed by soft X-ray. The relative radiographic density of the region was evaluated by image analysis. Micro computed tomography (μCT) examinations were used to determine the change in the trabecular bone. This was carried out by using a SkyScan1173 (SKYSCAN, Belgium) at 8 μm resolution. The degree of bone density on μCT was quantified by using the mean gray value and standard deviation of the region of interest (ROI). All morphometric parameters were obtained by using On-demand software (CyberMed Inc., Korea). After μCT analysis, the femora of each animal was removed and stained with hematoxylin and eosin (H&E) for histological analysis.

Statistical Analysis. All values are expressed as means ± standard deviations. Statistical analysis was performed using PASW Statistics 21 software (SPSS, Inc., Chicago, IL). Multiple comparisons were analyzed using one-way analysis of variance (ANOVA) followed by Dunnett's T3 post hoc paired comparison test. A value of $p < 0.05$ is considered to be statistically significant.

Conflict of Interest: The authors declare no competing financial interest.

Acknowledgment. This research was supported by the Public Welfare & Safety research program through the National Research Foundation of Korea (NRF) funded by the Ministry of Education, Science and Technology (NRF-2012-0008610, NRF-2010-0019346, and NRF-2012R1A5A2051388).

Supporting Information Available: Additional figures of the loading efficiency of CUR in the CGNPs, body weight of ovariectomized mice during experimental period, relative femur weight, and average value of trabecular bone parameters in experimental groups. This material is available free of charge *via* the Internet at http://pubs.acs.org.

REFERENCES AND NOTES

1. Cho, E. C.; Glaus, C.; Chen, J.; Welch, M. J.; Xia, Y. Inorganic Nanoparticle-Based Contrast Agents for Molecular Imaging. *Trends Mol. Med.* **2010**, *16*, 561–573.
2. Ghosh, P.; Han, G.; De, M.; Kim, C. K.; Rotello, V. M. Gold Nanoparticles in Delivery Applications. *Adv. Drug. Delivery Rev.* **2008**, *60*, 1307–1315.
3. Kim, K.; Fisher, J. P. Nanoparticle Technology in Bone Tissue Engineering. *J. Drug Target.* **2007**, *15*, 241–252.
4. Yi, C.; Liu, D.; Fong, C.-C.; Zhang, J.; Yang, M. Gold Nanoparticles Promote Osteogenic Differentiation of Mesenchymal Stem Cells Through p38 MAPK Pathway. *ACS Nano* **2010**, *4*, 6439–6448.
5. Liu, D. D.; Zhang, J. C.; Yi, C. Q.; Yang, M. S. The Effects of Gold Nanoparticles on the Proliferation, Differentiation, and Mineralization Function of MC3T3-E1 Cells *in vitro*. *Chin. Sci. Bull.* **2010**, *55*, 1013–1019.
6. Ko, W.-K.; Heo, D. N.; Moon, H.-J.; Lee, S. J.; Bae, M. S.; Lee, J. B.; Sun, I.-C; Jeon, H. B.; Park, H. K.; Kwon, I. K. The Effect of Gold Nanoparticle Size on Osteogenic Differentiation of Adipose-Derived Stem Cells. *J. Colloid Interface Sci.* **2015**, *438*, 68–76.
7. Li, X.; Liu, H.; Niu, X.; Yu, B.; Fan, Y.; Feng, Q.; Cui, F.-Z.; Watari, F. The Use of Carbon Nanotubes to Induce Osteogenic Differentiation of Human Adipose-Derived MSCs *in vitro* and Ectopic Bone Formation *in vivo*. *Biomaterials* **2012**, *33*, 4818–4827.
8. Cheng, Q.; Rutledge, K.; Jabbarzadeh, E. Carbon Nanotube-Poly(lactide-co-glycolide) Composite Scaffolds for Bone Tissue Engineering Applications. *Ann. Biomed. Eng.* **2013**, *41*, 904–916.
9. Akhavan, O.; Ghaderia, E.; Shahsavar, M. Graphene Nanogrids for Selective and Fast Osteogenic Differentiation of Human Mesenchymal Stem Cells. *Carbon* **2013**, *59*, 200–211.
10. Yang, K.; Cao, W.; Hao, X.; Xue, X.; Zhao, J.; Liu, J.; Zhao, Y.; Meng, J.; Sun, B.; Zhang, J.; et al. Metallofullerene Nanoparticles Promote Osteogenic Differentiation of Bone Marrow Stromal Cells Through BMP Signaling Pathway. *Nanoscale* **2013**, *5*, 1205–1212.
11. Sul, O.-J.; Kim, J.-C.; Kyung, T.-W.; Kim, H.-J.; Kim, Y.-Y.; Kim, S.-H.; Kim, J.-S.; Choi, H.-S. Gold Nanoparticles Inhibited the Receptor Activator of Nuclear Factor-κb Ligand (RANKL)-Induced Osteoclast Formation by Acting as an Antioxidant. *Biosci. Biotechnol. Biochem.* **2010**, *74*, 2209–2213.
12. Kim, W.-K.; Kim, J.-C.; Park, H.-J.; Sul, O.-J.; Lee, M.-H.; Kim, J.-S.; Choi, H.-S. Platinum Nanoparticles Reduce Ovariectomy-Induced Bone Loss by Decreasing Osteoclastogenesis. *Exp. Mol. Med.* **2012**, *44*, 432–439.
13. Beck, G. R., Jr.; Ha, S. W.; Camalier, C. E.; Yamaguchi, M.; Li, Y.; Lee, J. K.; Weitzmann, M. N. Bioactive Silica-Based Nanoparticles Stimulate Bone-Forming Osteoblasts, Suppress Bone-Resorbing Osteoclasts, and Enhance Bone Mineral Density *in vivo*. *Nanomedicine* **2012**, *8*, 793–803.
14. Boyle, W. J.; Simonet, W. S.; Lacey, D. L. Osteoclast Differentiation and Activation. *Nature* **2003**, *423*, 337–342.
15. Teitelbaum, S. L. Bone Resorption by Osteoclasts. *Science* **2000**, *289*, 1504–1508.
16. Sperling, R. A.; Gil, P. R.; Zhang, F.; Zanella, M.; Parak, W. J. Biological Applications of Gold Nanoparticles. *Chem. Soc. Rev.* **2008**, *37*, 1896–1908.
17. Giljohann, D. A.; Seferos, D. S.; Daniel, W. L.; Massich, M. D.; Patel, P. C.; Mirkin, C. A. Gold Nanoparticles for Biology and Medicine. *Angew. Chem., Int. Ed.* **2010**, *49*, 3280–3294.
18. Dykman, L.; Khlebtsov, N. Gold Nanoparticles in Biomedical Applications: Recent Advances and Perspectives. *Chem. Soc. Rev.* **2012**, *41*, 2256–2282.
19. Heo, D. N.; Yang, D. H.; Moon, H.-J.; Lee, J. B.; Bae, M. S.; Lee, S. C.; Lee, W. J.; Sun, I.-C.; Kwon, I. K. Gold Nanoparticles Surface-Functionalized with Paclitaxel Drug and Biotin Receptor as Theranostic Agents for Cancer Therapy. *Biomaterials* **2012**, *33*, 856–866.
20. Arima, H.; Yamashita, S.; Mori, Y.; Hayashi, Y.; Motoyama, K.; Hattori, K.; Takeuchi, T.; Jono, H.; Ando, Y.; Hirayama, F.; *et al. in vitro* and *in vivo* Gene Delivery Mediated by Lactosylated Dendrimer/α-Cyclodextrin Conjugates (G2) into Hepatocytes. *J. Controlled Release* **2010**, *146*, 106–117.
21. Shu, S.; Zhang, X.; Wu, Z.; Wang, Z.; Li, C. Gradient Cross-Linked Biodegradable Polyelectrolyte Nanocapsules for Intracellular Protein Drug Delivery. *Biomaterials* **2010**, *31*, 6039–6049.
22. Jeong, S.-Y.; Park, S.-J.; Yoon, S. M.; Jung, J.; Woo, H. N.; Yi, S. L.; Song, S. Y.; Park, H. J.; Kim, C.; Lee, J. S.; *et al.* Systemic Delivery and Preclinical Evaluation of Au Nanoparticle Containing β-lapachone for Radiosensitization. *J. Controlled Release* **2009**, *139*, 239–245.
23. Yadav, V. R.; Suresh, S.; Devi, K.; Yadav, S. Effect of Cyclodextrin Complexation of Curcumin on its Solubility and Antiangiogenic and Anti-Inflammatory Activity in Rat Colitis Model. *AAPS PharmSciTech* **2009**, *10*, 752–762.
24. Maheshwari, R. K.; Singh, A. K.; Gaddipati, J.; Srimal, R. C. Multiple Biological Activities of Curcumin: A Short Review. *Life Sci.* **2006**, *78*, 2081–2087.
25. Wilken, R.; Veena, M. S.; Wang, M. B.; Srivatsan, E. S. Curcumin: A Review of Anti-Cancer Properties and Therapeutic Activity in Head and Neck Squamous Cell Carcinoma. *Mol. Cancer* **2011**, *10*, 12.
26. Baglole, K. N.; Boland, P. G.; Wagner, B. D. Fluorescense Enhancement of Curcumin upon Inclusion into Parent and Modified Cyclodextrins. *J. Photochem. Photobiol., A* **2005**, *173*, 230–237.
27. Yallapu, M. M.; Jaggi, M.; Chauhan, S. C. β-Cyclodextrin-Curcumin Self-Assembly Enhances Curcumin Delivery in Prostate Cancer Cells. *Colloids Surf. B Biointerfaces* **2010**, *79*, 113–125.
28. Yallapu, M. M.; Jaggi, M.; Chauhan, S. C. Poly-(β-Cyclodextrin)/Curcumin Self-Assembly: a Novel Approach to Improve Curcumin Delivery and Its Therapeutic Efficacy in Prostate Cancer Cells. *Macromol. Biosci.* **2010**, *10*, 1141–1151.

29. Anand, P.; Nair, H. B.; Sung, B.; Kunnumakkara, A. B.; Yadav, V. R.; Tekmal, R. R.; Aggarwal, B. B. Design of curcumin-loaded PLGA nanoparticles formulation with enhanced cellular uptake, and increased bioactivity *in vitro* and superior bioavailability *in vivo*. *Biochem. Pharmacol.* **2010**, *79*, 330–338.
30. Bharti, A. C.; Takada, Y.; Aggarwal, B. B. Curcumin (Diferuloylmethane) Inhibits Receptor Activator of NF-κB Ligand-Induced NF-κB Activation in Osteoclast Precursors and Suppresses Osteoclastogenesis. *J. Immunol.* **2004**, *172*, 5940–5947.
31. Moon, H.-J.; Ko, W.-K.; Han, S. W.; Kim, D.-S.; Hwang, Y.-S.; Park, H.-K.; Kwon, I. K. Antioxidants, like Coenzyme Q10, Selenite, and Curcumin, Inhibited Osteoclast Differentiation by Suppressing Reactive Oxygen Species Generation. *Biochem. Biophys. Res. Commun.* **2012**, *418*, 247–253.
32. Tomren, M. A.; Másson, M.; Loftsson, T.; Tønnesen, H. H. Studies on Curcumin and Curcuminoids XXXI. Symmetric and Asymmetric Curcuminoids: Stability, Activity and Complexation with Cyclodextrin. *Int. J. Pharm.* **2007**, *338*, 27–34.
33. Tønnesen, H. H.; Másson, M.; Loftsson, T. Studies of Curcumin and Curcuminoids. XXVII. Cyclodextrin Complexation: Solubility, Chemical and Photochemical Stability. *Int. J. Pharm.* **2002**, *244*, 127–135.
34. Tang, B.; Ma, L.; Wang, H.-Y.; Zhang, G.-Y. Study on the Supramolecular Interaction of Curcumin and β-Cyclodextrin by Spectrophotometry and Its Analytical Application. *J. Agric. Food Chem.* **2002**, *50*, 1355–1361.
35. Dubertret, B.; Calame, M.; Libchaber, A. J. Single-Mismatch Detection Using Gold-Quenched Fluorescent Oligonucleotides. *Nat. Biotechnol.* **2001**, *19*, 365–370.
36. Boyce, B. F.; Yamashita, T.; Yao, Z.; Zhang, Q.; Li, F.; Xing, L. Roles for NF-κB and c-Fos in Osteoclasts. *J. Bone Miner. Metab.* **2005**, *23*, 11–15.
37. Takayanagi, H.; Kim, S.; Koga, T.; Nishina, H.; Isshiki, M.; Yoshida, H.; Saiura, A.; Isobe, M.; Yokochi, T.; Inoue, J.; *et al.* Induction and Activation of the Transcription Factor NFATc1 (NFAT2) Integrate RANKL Signaling in Terminal Differentiation of Osteoclasts. *Dev. Cell* **2002**, *3*, 889–901.
38. Moon, H.-J.; Kim, E.-K.; Nam, Y. S.; Kim, J. H.; Ko, W.-K.; Lee, J.-M.; Lee, C.-H.; Jang, J.-B.; Lee, K.-S.; Kwon, I. K. Safflower Seed Extract Inhibits Osteoclast Differentiation by Suppression of the p38 Mitogen-Activated Protein Kinase and IκB Kinase Activity. *Phytother. Res.* **2012**, *26*, 1648–1655.
39. Hwang, Y. H.; Lee, J. W.; Hahm, E.-R.; Jung, K. C.; Lee, J. H.; Park, C. H.; Rhee, H. S.; Ryu, J. M.; Kim, H.-K.; Yang, C.-H. Momordin I, an Inhibitor of AP-1, Suppressed Osteoclastogenesis Through Inhibition of NF-κB and AP-1 and also Reduced Osteoclast Activity and Survival. *Biochem. Biophys. Res. Commun.* **2005**, *337*, 815–823.
40. Ha, H.; Kwak, H. B.; Lee, S. W.; Jin, H. M.; Kim, H.-M.; Kim, H.-H.; Lee, Z. H. Reactive Oxygen Species Mediate RANK Signaling in Osteoclasts. *Exp. Cell Res.* **2004**, *301*, 119–127.
41. Lee, Z. H.; Lee, S. E.; Kim, C.-W.; Lee, S. H.; Kim, S. W.; Kwack, K.; Walsh, K.; Kim, H.-H. IL-1α Stimulation of Osteoclast Survival Through the PI 3-Kinase/Akt and ERK Pathways. *J. Biochem.* **2002**, *131*, 161–166.
42. Stadelmann, V. A.; Gauthier, O.; Terrier, A.; Bouler, J. M.; Pioletti, D. P. Implants delivering bisphosphonate locally increase periprosthetic bone density in an osteoporotic sheep model. A pilot study. *Eur. Cell. Mater.* **2008**, *16*, 10–16.
43. Josse, S.; Faucheux, C.; Soueidan, A.; Grimandi, G.; Massiot, D.; Alonso, B.; Janvier, P.; Laïb, S.; Pilet, P.; Gauthier, O.; *et al.* Novel biomaterials for bisphosphonate delivery. *Biomaterials* **2005**, *26*, 2073–2080.
44. Walter, C.; Al-Nawas, B.; Grötz, K. A.; Thomas, C.; Thüroff, J. W.; Zinser, V.; Gamm, H.; Beck, J.; Wagner, W. Prevalence and risk factors of bisphosphonate-associated osteonecrosis of the jaw in prostate cancer patients with advanced disease treated with zoledronate. *Eur. Urol.* **2008**, *54*, 1066–1072.
45. Zhang, X. D.; Wu, D.; Shen, X.; Liu, P. X.; Yang, N.; Zhao, B.; Zhang, H.; Sun, Y. M.; Zhang, L. A.; Fan, F. Y. Size-dependent *in vivo* toxicity of PEG-coated gold nanoparticles. *Int. J. Nanomed.* **2011**, *6*, 2071–2081.
46. Heo, D. N.; Ko, W.-K.; Bae, M. S.; Lee, J. B.; Lee, D.-W.; Byun, W.; Lee, C. H.; Kim, E.-C.; Jung, B.-Y.; Kwon, I. K. Enhanced bone regeneration with a gold nanoparticle–hydrogel complex. *J. Mater. Chem. B* **2014**, *2*, 1584–1593.
47. Lee, S. E.; Woo, K. M.; Kim, S. Y.; Kim, H.-M.; Kwack, K.; Lee, Z. H.; Kim, H.-H. The Phosphatidylinositol 3-Kinase, p38, and Extracellular Signal-Regulated Kinase Pathways Are Involved in Osteoclast Differentiation. *Bone* **2002**, *30*, 71–77.
48. Javeri, A.; Lyons, J. G.; Huang, X. X.; Halliday, G. M. Down-regulation of Cockayne syndrome B protein reduces human 8-oxoguanine DNA glycosylase-1 expression and repair of UV radiation-induced 8-oxo-7,8-dihydro-2′-deoxyguanine. *Cancer Sci.* **2011**, *102*, 1651–1658.